Voltage-dependent capacitance of human embryonic kidney cells

Brenda Farrell,* Cythnia Do Shope, and William E. Brownell
Department of Otolaryngology and Head and Neck Surgery, Baylor College of Medicine Houston, Texas 77030, USA
(Received 21 October 2004; revised manuscript received 26 July 2005; published 28 April 2006; corrected 12 May 2006)

We determine membrane capacitance, C as a function of dc voltage for the human embryonic kidney (HEK) cell. C was calculated from the admittance, Y, obtained during a voltage ramp when the HEK cell was held in whole-cell patch-clamp configuration. Y was determined at frequencies of 390.625 and 781.25 Hz from the measured current, i obtained with a dual-sinusoidal stimulus. We find that the fractional increase in the capacitance, C is small ($<1\%$) and grows with the square of the voltage, Ψ. C can be described by: $C=C(0)(1+\alpha(\Psi+\psi_s)^2)$ [where $C(0)$: Capacitance at 0 volts, ψ_s: Difference in surface potential between cytoplasmic and extracellular leaflets and α: Proportionality constant]. We find that α and ψ_s are 0.120 ($\pm$0.01) V^{-2} and -0.073 ($\pm$0.017) V in solutions that contain ion channel blockers and 0.108 ($\pm$0.29) V^{-2} and -0.023 ($\pm$0.009) V when 10 mM sodium salicylate was added to the extracellular solution. This suggests that salicylate does not affect the rate at which C grows with Ψ, but reduces the charge asymmetry of the membrane. We also observe an additional linear differential capacitance of about (-46 fFV^{-1}) in about 60% of the cells, this additional component acts simultaneously with the quadratic component and was not observed when salicylate was added to the solution. We suggest that the voltage dependent capacitance originates from electromechanical coupling either by electrostriction and/or Maxwell stress effects and estimate that a small electromechanical force ($\approx$1 pN) acts at physiological potentials. These results are relevant to understand the electromechanical coupling in outer hair cells (OHCs) of the mammalian cochlea, where an asymmetric bell-shaped C versus Ψ relationship is observed upon application of a similar field. Prestin, a membrane protein expressed in OHCs is required to observe this function. When we compare the total charge contributions from HEK cell membrane (7×10^4 electrons, 10 pF cell) with that determined for prestin transfected cells (up to 5×10^6 electrons) we conclude that the charge contributions from the collective motion of membrane proteins and lipids in the field is dwarfed relative to that when prestin is present. We suggest that the capacitance-voltage relationships should be similar to that observed for HEK cells for OHCs that do not express prestin in their membranes.

DOI: 10.1103/PhysRevE.73.041930 PACS number(s): 83.80.Lz, 43.64.+r

I. INTRODUCTION

Outer hair cell (OHC) electromotility is responsible for amplification of high frequency vibrations in the inner ear [1–3]. A significant force ($\approx$nN) is produced during OHC electromotility by electro-mechanical coupling [2,4–6]. Prestin, a membrane protein found in the membranes of OHCs [7], is essential for OHC electromechanical coupling [3]. To examine the functional expression of prestin it is common to transfect human embryonic kidney (HEK) cells or Chinese hamster ovary, CHO cells [8] with prestin to determine the response of the transfected cells to a varying electric field, E. Because the electrical response of the wildtype HEK cell to a varying E field is not fully characterized, we examined the response by measuring the capacitance, C as a function of the dc voltage in the presence of ionic channel blockers and when sodium channel gating currents were inactivated. We show that the fractional increase in C is small ($<1\%$) and grows with the square of the field ($C\propto E^2$). This is similar to that observed for lipid bilayers [9]. In many cells, (60%) we also observe an additional small linear decrease in the capacitance as the potential moves from negative to positive values, this additional component acts simultaneously with the quadratic component. This linear component was not observed in studies with lipid bilayers [9]. We suggest that both components arise from electromechanical coupling producing a small force ($\approx$pN) at physiological potentials.[1]

II. METHODS

A. Cells

Cells were grown in medium based on Dulbecco's modification of Eagle's medium (DMEM) (Mediatech, Herndon, VA). It contained in 1 L: 100 mL of fetal bovine serum (Invitrogen, Life Technology, Carlsbad, CA); 17.8 mM $NaHCO_3$ and 15.8 mM HEPES dissolved in DMEM. The HEK 293 cell line was purchased from American Type Cell Culture (Manassa, VA). Frozen cells (1 mL at 10^6 cells mL^{-1}) were suspended in 9 mL of DMEM and centrifuged slowly for 5 min. The cell pellet was resuspended in 10 mL of fresh media and plated in a 100 cm^3 culture flask (Beckton Dickinson, Franklin Lakes, NJ). The flasks were placed in a water-jacketed CO_2 incubator (Nuaire, Plymouth, MN) and maintained at 37 °C in 5% CO_2. HEK cells adsorb to the polystyrene surface and are about 90% confluent within one week. The cells were passed weekly where cells

*Corresponding author. Email address: bfarrell@bcm.edu

[1]A preliminary version of this work was presented at Biophysical Society meetings in San Antonio, TX February 2003 and Baltimore, MD February 2004.

used in the experiments were passed 15–25 times. Briefly, the excess media was decanted from the flask and 2 mL of trypsin at 10 mg of trypsin mL^{-1} of EDTA (Invitrogen Life Technology, Carlsbad, CA) was added and cells were incubated at 37 °C for 5 min. 8 mL of DMEM was then added to terminate the trypsin hydrolysis and the cell suspension was mechanically agitated. The concentration of cells was determined with a hemacytometer (Fisher Scientific, Hampton, NH) from an aliquot of the suspension. To pass the cells, an aliquot of this cell suspension was added to a fresh flask containing 10 mL of DMEM and placed in the incubator at a concentration of 5×10^5 cells mL^{-1}. For each experiment an aliquot of the dissociated cells (concentration of 2×10^4 cells mL^{-1}) was plated onto 10 mm glass bottom culture dishes coated with Poly-d-lysine (MatTek Corp. Ashland MA) and placed in the incubator at 37 °C for 2–18 h.

B. Whole cell patch clamping

All chemicals were purchased from Sigma-Aldrich (St Louis, M0) except sodium salicylate which was from Fluka (distributed by Sigma-Aldrich) and all were used without further purification. The solution within the pipette contained (in mM) 140 CsCl, 2 $MgCl_2$, 10 EGTA, and 10 HEPES and the extracellular solution contained (in mM) 100 NaCl, 20 CsCl, 20 N-$(CH_2CH_3)_4$ Cl, 10 HEPES, 2 $CoCl_2$, 1.47 $MgCl_2$, 2 $CaCl_2$. The pH and osmolality were adjusted to 7.2 (±0.02) and 300 (±2) mOsm Kg^{-1} with the addition of CsOH and glucose, respectively. The concentration of NaCl was reduced to maintain the osmolality at 300 mOsm Kg^{-1} when 10 mM sodium salicylate was added to the external medium. In some experiments, 1 mM $BaCl_2$ was added to the external medium as an additional block of potassium channels and once again the concentration of NaCl was reduced to maintain the osmolality at 300 mOsm Kg^{-1}. In other experiments 130 μM DIDS (4,4′-Diisothiocyanatostilbene-2′,2-disulfonic acid disodium salt) was added to the external medium to block chloride channels. DIDS was first dissolved in water and then dissolved in the extracellular solution. Most pipettes were made from fused quartz (Sutter Instrument Company, Novato, CA), a few were made from borosilicate glass (WPI, Sarasota, FL) and formed with a CO_2 laser-based micropipette puller (Sutter Instrument Company, Novato, CA). The pipettes were coated with Sylgard (Dow Corning, Midland, MI) and had a resistance between 2 and 3 Mohm.

The culture dish containing cells was placed on an inverted microscope (Carl Zeiss, Gottingen, Germany) and the growth medium was exchanged for the external solution by use of a peristaltic pump (RP-1 4 channel pump, Rainin, Oakland, CA). The flow rate was constant at about 4 mL min^{-1} and the solution was continuously perfused throughout the course of an experiment with the depth of the solution maintained at 1.0–1.5 mm. A single isolated cell was chosen for an experiment. Cell membrane admittance was measured with the patch-clamp technique in the whole-cell mode [Fig. 1(a)]. An electrical seal (>10 Gohm) was formed between the pipette and cell membrane then the pipette capacitance was corrected with the compensation circuitry of an amplifier (Axon 200B, Molecular Devices, Union City, CA). Typically the fast capacitance transients disappeared into the baseline noise after compensation, where root mean square noise was about ±0.5 pA. Once the cell was in the whole-cell mode at 0 mV the cell admittance was monitored during a dc voltage ramp. During a ramp the voltage increased at 0.3 Vs^{-1} from −0.16 to 0.16 V. Sometimes the polarity of the stimulus was reversed or the dc voltage was greater at ±0.17 V. The holding potential was 0 V before and after the ramp. Voltages were measured relative to a Ag/AgCl reference electrode. The admittance was probed with dual-frequency stimulus [10,11]. A dual-frequency stimulus was used because it permits the calculation of the membrane capacitance, C, membrane resistance, R_m and series resistance, R_s from the measured admittance during a dc voltage ramp. This method is not suitable when imaginary part of the admittance, $[\mathrm{Im}(Y)]$ changes rapidly with voltage, which is the case for mammalian outer hair cells. For these cells the membrane resistance cannot be determined from the admittance but must be determined independently at dc [12]. The stimulus was the sum of two 10 mV peak to peak sine waves at frequency, f of 390.625 Hz and $2f$, 781.25 Hz. The current, i was measured every 10 μs and a Fast Fourier Transform conducted every 512 or 1024 records to determine the real $\mathrm{Re}(i)$ and imagi-

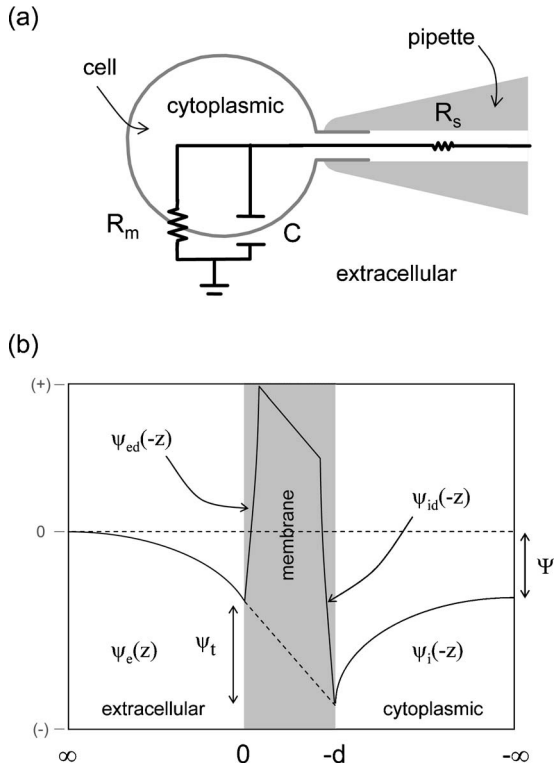

FIG. 1. (a) Schematic showing equivalent electrical circuit of cell under whole-cell voltage clamp. Where R_s: Series resistance; R_m: Membrane resistance, C: Membrane capacitance. (b) Definition of potentials, Ψ: Transmembrane potential, ψ_t: Potential difference across the membrane; $\psi_i(-z)$: Potential at cytoplasmic compartment; $\psi_e(z)$: Potential at extracellular compartment; $\psi_{id}(-z)$: Dipole potential at cytoplasmic side; $\psi_{ed}(-z)$: Dipole potential at extracellular side.

nary, Im(i) parts of the current, (i) every 5.12 or 10.24 ms at each frequency. This current was first corrected for the inherent phase shifts of the amplifier and then the Re(Y) and Im(Y) parts of the admittance, Y were calculated by dividing the complex current by the complex voltage. Before an experiment the software was calibrated for amplifier shifts by use of a 10 Mohm resistor as described [11]. A computer program written in LABVIEW (v6.1) for Windows in conjunction with a digital to analog converter card (AT-MIO-16XE-10, National Instruments Austin, TX) controlled the calibration, stimulus, and acquisition of the admittance. In some experiments the conductance was also determined experimentally with a dc protocol, where the voltage was ramped from −0.16 to 0.16 V. Briefly, a square wave pulse with an amplitude of 0.01 V was applied to the cell via the pipette. The current was sampled every 10 or 100 μs for a 1000 times (400 points before pulse, 500 points during the pulse, and 100 points after the pulse) at each voltage. The longer sampling times were used to determine the conductance of cells with high resistance (>4 Gohm), where the conductance was then calculated from the change in the steady-state part of the measured current relative to the change in the voltage. In some experiments the current versus voltage plot was determined. The voltage was ramped from −0.13 to +0.13 V in 0.01 V steps, and current was sampled every 100 μs a 1000 times at each voltage. The reversal potential was determined from the plot, it is the voltage when the ionic flux across the membrane is zero.

C. Definition of potentials

Our objective is to determine the membrane capacitance, C as a function of voltage, it is therefore pertinent to clarify the potentials in the system. The transmembrane potential, Ψ is

$$\Psi \equiv \psi_i(-\infty) - \psi_e(\infty) \equiv \psi_i(-\infty) \tag{2.1}$$

where $\psi_i(-\infty)$ and $\psi_e(\infty) \equiv 0$ are the potentials in the bulk at the cytoplasmic and extracellular compartments of the cell, respectively (Fig. 1). This arises because each ion permeates the membrane at a different rate and each ion is present at different concentrations in each compartment. The voltage applied to the cytoplasmic solution from the amplifier via the pipette is Ψ [Fig. 1(a)]. For our analysis we assume the applied potential to be equivalent to Ψ. This is a reasonable assumption because the magnitude of the drop across the pipette is very small (<0.02%). In Fig. 1(b) we also show the surface potentials at the cytoplasmic, $\psi_i(-d) - \psi_i(-\infty)$ and extracellular, $\psi_e(0)$ interfaces for a membrane of thickness, d where the difference between them is

$$\psi_s = \psi_i(-d) - \Psi - \psi_e(0). \tag{2.2}$$

The surface potentials arise from the intrinsic surface charge at each leaflet of the membrane. Cell membranes are asymmetric with respect to charge and chemical composition with the inner leaflet more negatively charged than the outer leaflet [13]. The dipole potentials at the cytoplasmic $\psi_{id}(-z) - \psi_i(-\infty)$ and extracellular parts of the membrane $\psi_{ed}(-z)$ are also shown in Fig. 1(b). They arise from the structural organization of polar molecules at the membrane-water interfaces. Finally, the potential difference across the membrane, ψ_t is defined as:

$$\psi_t = \psi_i(-d) - \psi_e(0). \tag{2.3}$$

D. Cell parameters

We use two algorithms to calculate the capacitance C, membrane resistance, R_m and series resistance, R_s as a function of voltage, Ψ [Fig. 1(a)]. The first method is similar to that described [10] and similar to that first outlined by others [14]. Briefly, provided the dc cell conductance, $b(\Psi) = 1/[R_m(\Psi) + R_s(\Psi)]$ at $f = 0$, is known the cell parameters can be calculated at Ψ and at frequency, f from the admittance $Y(f,\Psi) = \mathrm{Re}(Y,\Psi) + j\,\mathrm{Im}(Y,\Psi)$ with:

$$R_s(\Psi) = \frac{(A - b(\Psi))}{(A^2 + B^2 - Ab(\Psi))},$$

$$R_m(\Psi) = \frac{(A - b(\Psi))^2 + B^2}{b(\Psi)(A^2 + B^2 - Ab(\Psi))}$$

$$C(\Psi) = \frac{1}{2\pi f B} \frac{(A^2 + B^2 - Ab)^2}{((A - b(\Psi))^2 + B^2)} \tag{2.4}$$

where

$$A = \mathrm{Re}(Y,\Psi) = \frac{R_s + R_m + (2\pi f)^2 C^2 R_m^2 R_s}{((R_s + R_m)^2 + (2\pi f)^2 C^2 R_m^2 R_s^2)},$$

$$B = \mathrm{Im}(Y,\Psi) = \frac{j 2\pi f C R_m^2}{((R_s + R_m)^2 + (2\pi f)^2 C^2 R_m^2 R_s^2)} \tag{2.5}$$

and $j = (-1)^{0.5}$.

$b(\Psi)$ was determined by re-writing the first term of (2.4) in terms of $b(\Psi)$, equating the equations at each frequency and substituting the measured $\mathrm{Re}(Y,\Psi)$ and $\mathrm{Im}(Y,\Psi)$ parts at each frequency into the expression. In this case we note that $b(\Psi)$ calculated in this way is not exactly the same as $b(\Psi)$ determined at dc, and the estimate worsens as f increases, because from (2.5) when $R_m \gg R_s$ and $f \to 0$ then $\mathrm{Re}(Y) \to 1/R_m$, and for $f \to \infty$, then $\mathrm{Re}(Y) \to 1/R_s$. Once $b(\Psi)$ is estimated $R_s(\Psi)$, $R_m(\Psi)$, and $C(\Psi)$ are then readily estimated. Where we note that two values of $C(\Psi)$, are calculated, one at f, $C_f(\Psi)$ and one at $2f$, $C_{2f}(\Psi)$. We coin this *algorithm one* to distinguish it from the method outlined in [10] that calculates the average of the two capacitances. In some experiments $b(\Psi)$ was determined experimentally with a dc protocol. $C(\Psi)$ was the same (within a few fF) for both HEK cells and model circuits when it was calculated with $b(\Psi)$ determined experimentally with a dc protocol or with $b(\Psi)$ calculated directly from the equations by use of the admittance measurements.

A more sophisticated algorithm for calculating the cell parameters with dual-frequency sinusoidal stimulus was described [11]. It uses a nonlinear weighted least-squares approach to estimate the transfer coefficients and weights the

TABLE I. Electrical parameters of model circuits calculated from the measured admittance (second to sixth columns) or at dc (last two columns). Parameters calculated from the admittance were determined with *algorithm one* and *Barnett's algorithm*. R_m determined from dc algorithm was obtained by sampling the current every 10 μs (column 7) and 100 μs (column 8) at each voltage. The nominal R_s was 4(±1%) MΩ and nominal R_m was 10(±5%) (a) and 1(±1%) (b) GΩ. The nominal C is accurate to about ±5% for each capacitor, except for the 2 and 8 pF capacitors, which are accurate to about ±25 and 6.25%, respectively. The values obtained from admittance and for R_m determined at dc are average of 214 and 109 points, respectively. Coefficient of variation (standard deviation/mean×100) is in brackets.

Nominal Capacitance	C_f	C_{2f}	R_s	R_m	R_{mb}[a]	R_{mDC}	R_{mDC}
(a)	(pF)				(mΩ)		
2	3.372 (0.218)	3.354 (0.140)	4.74 (2.85)	5846 (15)	5717 (15)	9153 (29)	9216 (10)
8	8.851 (0.088)	8.820 (0.070)	4.53 (0.45)	2766 (7)	2639 (7)	5209 (15)	9390 (16)
15	15.817 (0.069)	15.796 (0.028)	4.27 (0.26)	6979 (29)	6081 (24)	12833 (50)	9873 (21)
18	18.991 (0.054)	18.960 (0.057)	4.25 (0.20)	4449 (20)	3852 (18)	28015 (362)	9688 (20)
22	22.736 (0.059)	22.708 (0.059)	4.21 (0.15)	5123 (28)	4276 (23)	63679 (734)	9613 (22)
30	30.296 (0.055)	30.248 (0.055)	4.15 (0.13)	6699 (48)	4278 (33)		9823 (18)
(b)							
2	2.412 (0.296)	2.396 (0.177)	7.70 (3.39)	879 (2.1)	876 (2.1)	993 (3)	1002 (1)
8	8.990 (0.090)	8.983 (0.066)	4.31 (0.54)	980 (2.8)	976 (2.7)	1007 (4)	999 (2)
15	16.204 (0.072)	16.158 (0.060)	4.26 (0.25)	860 (3.1)	829 (3.1)	1033 (4)	1006 (2)
18	19.185 (0.064)	19.178 (0.053)	4.25 (0.20)	904 (3.9)	898 (4.0)	1023 (4)	996 (2)
22	22.343 (0.061)	22.340 (0.055)	4.24 (0.18)	972 (4.4)	980 (4.7)	1109 (4)	999 (2)
30	30.158 (0.053)	30.185 (0.057)	4.20 (0.12)	1053 (5.4)	981 (4.8)	1369 (6)	997 (2)

[a]Membrane resistance calculated with Barnett's algorithm.

thermal noise introduced by the resistive cell components at each frequency. It does this because the resistive elements [R_m and R_s, Fig. 1(a)] are largely responsible for the thermal noise in the recordings. There are no reports of this algorithm being used to estimate cell parameters during a dc voltage ramp, we examined it to determine if it provided more accurate estimates than *algorithm one*. Briefly, the $\mathrm{Re}(Y,\Psi)$ and $\mathrm{Im}(Y,\Psi)$ parts of the admittance are written in terms of the transfer function coefficients $(a_1(\Psi), b_0(\Psi), b_1(\Psi))$ and at each frequency f and $2f$ are

$$\mathrm{Re}(Y_f,\Psi) + j\,\mathrm{Im}(Y_f,\Psi) = \frac{b_o(\Psi) + (2\pi f)^2 a_1(\Psi) b_1(\Psi)}{1 + (2\pi f)^2 (a_1(\Psi))^2} + j\frac{2\pi f (b_1(\Psi) - a_1(\Psi) b_o(\Psi))}{(1 + (2\pi f)^2 (a_1(\Psi))^2)} \tag{2.6}$$

$$\mathrm{Re}(Y_{2f},\Psi) + j\,\mathrm{Im}(Y_{2f},\Psi) = \frac{b_o(\Psi) + (4\pi f)^2 a_1(\Psi) b_1(\Psi)}{1 + (4\pi f)^2 (a_1(\Psi))^2} + j\frac{4\pi f (b_1(\Psi) - a_1(\Psi) b_o(\Psi))}{(1 + (4\pi f)^2 (a_1(\Psi))^2)}. \tag{2.7}$$

Once the transfer coefficients are found the cell parameters are readily calculated with

$$R_s(\Psi) = \frac{a_1(\Psi)}{b_1(\Psi)}, \quad R_m(\Psi) = \frac{(b_1(\Psi) - a_1(\Psi) b_o(\Psi))}{b_o(\Psi) b_1(\Psi)},$$

$$C(\Psi) = \frac{(b_1(\Psi))^2}{(b_1(\Psi) - a_1(\Psi) b_o(\Psi))}. \tag{2.8}$$

This algorithm is coined *Barnett's algorithm*. We tested it with their program (NWLS) which was written in MATLAB (Mathworks Inc, Natick MA).

E. Accuracy and precision of cell parameter estimates

To determine the accuracy of the parameter estimates we calculated cell parameters for model circuits [Fig. 1(a)] with electrical components similar in magnitude to those observed for HEK cells. Namely, C between 5 and 20 pF, R_m between 2 and 10 Gohm and R_s between 4 and 8 Mohm. Some of the results are outlined in Table I. We only show the capacitance and R_s values calculated with *algorithm one*. We found that the capacitance values calculated with *Barnett's algorithm* were of the same magnitude and noise level as those determined with *algorithm one* at the higher frequency $2f$. The R_s calculated with *Barnett's algorithm* also exhibited the same noise level and trends, although the magnitude was slightly less with *Barnett's algorithm* than that observed with *algorithm one*. In all cases the cell parameters were constant with voltage. The estimates of C are accurate to within 5%–10% over the range of interest, the noise is reasonable with the average value deviating by 0.07% from the mean value. The

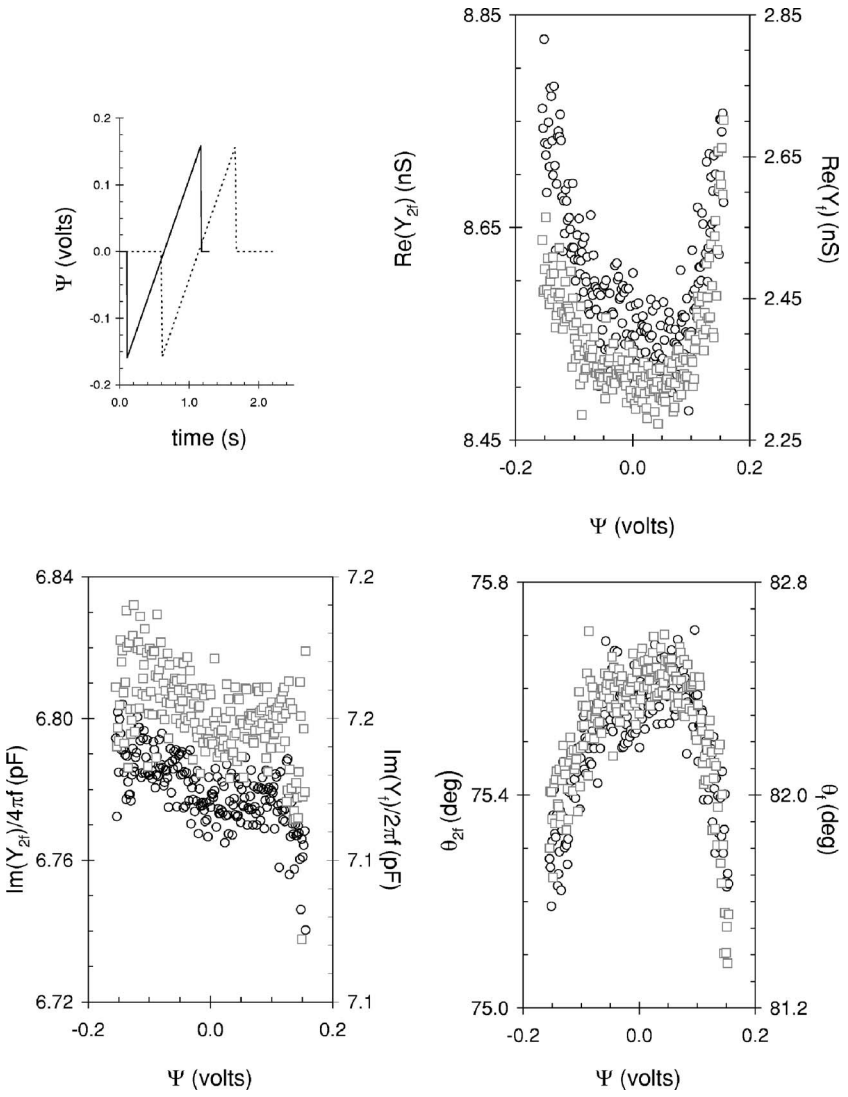

FIG. 2. Real, imaginary and phase of the admittance measured during a dc ramp when a HEK cell was held under whole-cell voltage clamp. The open circles and open gray squares represent the real part, imaginary part plotted as capacitance, and phase, of the admittance determined at $2f$ and f, i.e., 781.25 and 390.625 Hz, respectively. Note the different ordinates on each plot. The inset shows the time course of the dc stimulus (solid line) used to obtain the data, and dashed line shows a second dc stimulus. This second stimulus was introduced to estimate thermal drift, where current was measured for 0.6 s before and 0.55 s after the ramp with a total stimulus time of about 2.23 s.

estimates of R_s are also fairly accurate, values are within 5%–7% deviating by 0.4% from the mean value. In contrast, estimates of R_m at 10 Gohm are very inaccurate and underestimate it by 30%–70%. The membrane resistance is also noisy, and deviates by 10% from the mean for a 8 pF capacitor to about 35% for a 22 pF capacitor. In addition, estimates of R_m become even noisier as the R_s increases to 10 Mohm. For example, the R_m deviates by 100% from the mean for a 22 pF capacitor in parallel with a 10 Gohm resistor which are both in series with a 10 Mohm resistor. Similar trends are observed with 1 Gohm resistor, except in this case estimates of R_m are reasonable within 2%–15% with precision better at 5%. We found that the accuracy of the resistance was reasonable for circuits with R_m up to 2 Gohms, but was very inaccurate (off by 60%) for nominal resistances >4 Gohms with the noise tending to increase as the capacitance increased. Therefore, when $R_m > 2$ Gohms it is likely that both algorithms underestimate the true value at the stimulus frequencies of 390.625 and 781.25 Hz. When accurate estimates of R_m or b are required they should be measured directly with a dc protocol, where longer time pulses (100 ms cf. 10 ms) may be required to achieve reasonable estimates for cells or circuits that exhibit low conductances (Table I). Finally, it is apparent from Eq. (2.5) that as $f \to 0$ and $R_m \gg R_s$ the measured capacitance, $\frac{\mathrm{Im}(Y)}{2\pi f}$ approaches the actual capacitance of the circuit. This would suggest that the best estimate for C should be at a low frequency, this is not the case because thermal and especially flicker or pink noise contribute to the signal at low frequency [15]. Because of this noise the calculated capacitance (Table I) is different at both frequencies, where the optimum frequency to estimate the capacitance depends upon many factors including magnitude of the cell parameters, the amplitude of the sinusoidal stimulus, and the number of sinusoids used to estimate the capacitance [11,15].

III. RESULTS

A. Comparison of cell parameters calculated with *algorithm one* and *Barnett's algorithm*

Typical plots showing the real and imaginary components of the admittance for a HEK cell as a function of dc voltage at frequencies $f=390.625$ Hz and $2f=781.25$ Hz are shown in Fig. 2. The plots are for a single ramp from −0.16 to 0.16 V (see inset of Fig. 2). The $\mathrm{Re}(Y_f)$, $\mathrm{Re}(Y_{2f})$

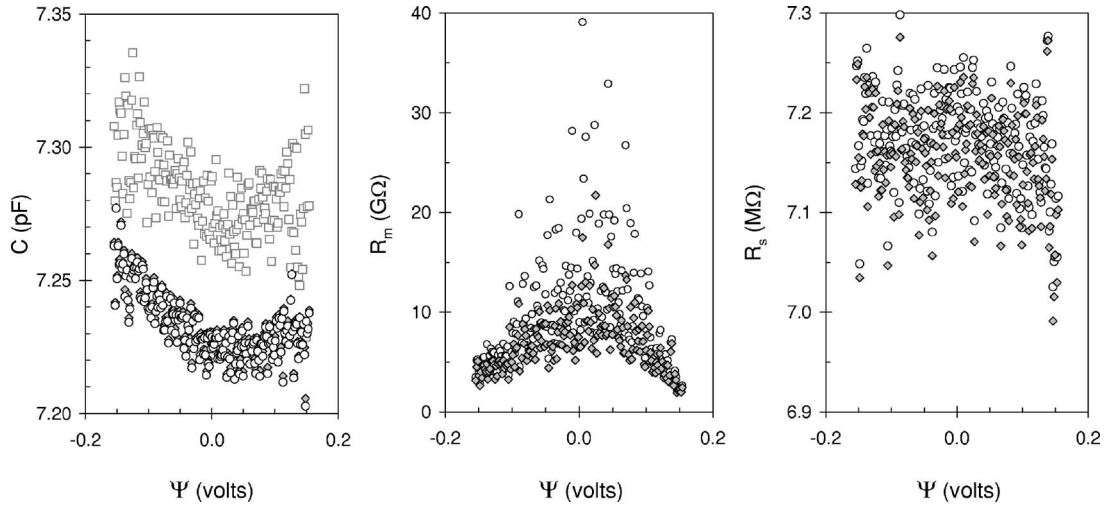

FIG. 3. The cell parameters calculated from the data in Fig. 2. Where open circles and open gray squares represent parameters calculated with *algorithm one* at frequencies of 781.25 and 390.625 Hz, respectively. The solid diamonds represent parameters calculated with *Barnett's algorithm*.

exhibit a parabolic shape with a minimum centered at 0 to 0.015 V. The $\mathrm{Im}(Y_f)/(2\pi f)$, $\mathrm{Im}(Y_{2f})/(4\pi f)$ decrease monotonically as the voltage extends from negative (hyperpolarizing) to positive (depolarizing) values. The phase, $\theta(Y_f)$ and $\theta(Y_{2f})$ at f and $2f$ are also shown in Fig. 2 and are parabolic with Ψ with a maximum centered at 0–0.01 V.

Shown in Fig. 3 are the cell parameters calculated from the admittance data outlined in Fig. 2. They were calculated with *algorithm one* (open circles and open squares) and *Barnett's algorithm* (filled diamonds). There is very little difference (up to 1.5 fF) in the C calculated at the higher frequency, $2f$ with *algorithm one* (open circles, left panel, Fig. 3) and that calculated with *Barnett's algorithm* (filled diamonds, left panel, Fig. 3). There are significant differences (up to 100 fF) when C is calculated at f as opposed to $2f$ with *algorithm one*. There is also a significant difference when C is calculated at f with *algorithm one* (open gray squares, left panel, Fig. 3) and when it is determined with *Barnett's algorithm*. In addition, the C calculated at f is noisier than that determined at $2f$ or with *Barnett's algorithm*. For both, C is parabolic with Ψ exhibiting a minimum around 0.05–0.06 V.

The R_m calculated with both algorithms exhibits a similar trend with voltage; it increases monotonically from −0.16 to 0 V and then decreases monotonically as the voltage becomes more positive (Fig. 3, middle panel). In addition, the R_m at the extreme positive potentials is about 1.5 Gohms less than that observed at the extreme negative potentials. The R_m determined with *Barnett's algorithm* (filled diamonds) is significantly less (from 0.2 to 2 Gohm) than that determined with *algorithm one* (open circles, middle panel, Fig. 3). It is also less noisier.

R_s (Fig. 3, right panel) is constant with voltage. The values determined with both algorithms exhibit similar noise with the value determined with *Barnett's algorithm* (filled diamonds) slightly less at up to 0.04 Mohm. The trends shown in Fig. 3 were the same if the stimulus was reversed, i.e., from 0.16 to −0.16 V and were also typical for other HEK cells that exhibited a good seal (>10 Gohm) and high resistance ($R_m > 2$ Gohm) at the extreme voltages with much higher resistance ($R_m \approx 4-10$ Gohm) at the middle of the voltage range.

We conclude that *Barnett's algorithm* provides the better method for determining cell estimates for a varying dc voltage because it automatically finds the solution of lowest noise from the experimental admittance. However, we note for voltage dependent capacitance of HEK cells that both methods provide the same result provided the C estimates are taken at the better frequency, which in this case is at 781.25 Hz.

B. Membrane capacitance is a function of voltage

Outlined in Fig. 4(a) is a plot of C versus Ψ for data obtained from the same cell shown in Figs. 2 and 3. The plot is the average of five dc ramps which reduces the noise. C is quadratic with Ψ. We only show plots calculated with *algorithm one*, and we show the results at both frequencies to illustrate that the quadratic relationship is evident in both of them. We do not show the results for the C with *Barnett's algorithm* because it is the same as that calculated with *algorithm one* at the higher frequency.

When the applied voltage is small (<1 V) $C(\Psi)$ can be described by

$$C(\Psi) \approx C(0)(1 + \alpha(\psi_t)^2)$$

which by use of (2.2) and (2.3) can be rewritten as

$$C(\Psi) \approx C(0)(1 + \alpha(\psi_s + \Psi)^2) \tag{3.1}$$

where $C(0)$ is the capacitance at zero volts, and α is a proportionality constant [16]. It is evident that $(dC)/(d\Psi)=0$ when $\Psi=-\psi_s$, and the minimum value of C occurs when the applied voltage is the same magnitude, but of opposite polarity to the difference in surface potentials. ψ_s is calculated

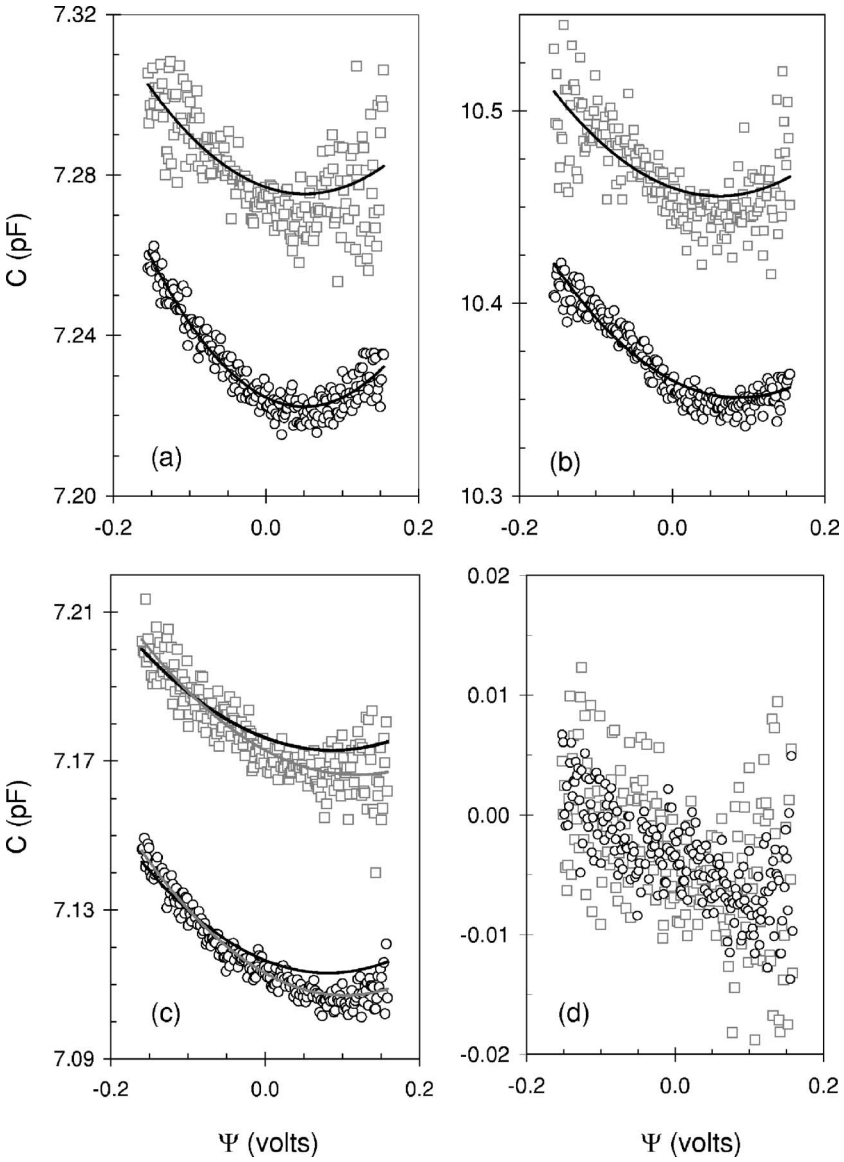

FIG. 4. Capacitance-voltage relationships determined for three HEK cells. The symbols are defined in Fig. 3. (a) The black solid lines are a fit of the data to Eq. (3.1) where α and ψ_s are 0.089 V^{-2} and −0.051 V (upper plot) and 0.126 V^{-2} and −0.0505 V (lower plot), respectively. 202 data points (N) were used to make the fit with the residual sum of squares calculated to be 0.0143 (upper) and 0.0022 (lower). (b) Same as (a) where α and ψ_s are 0.108 V^{-2} and −0.078 V (upper plot) and 0.135 V^{-2} and −0.075 V (lower plot), respectively. Residual sum of squares are 0.056 (upper) and 0.009 (lower) (N=202). The data is the average of 2 dc ramps. (c) Same as (a) where α and ψ_s are 0.062 V^{-2} and −0.087 V (upper plot) and 0.072 V^{-2} and −0.081 V (lower plot), respectively. The residual sum of squares are 0.011 (upper) and 0.006 (lower) (N=208). The solid gray line is a fit to Eq. (3.2) where α, α_1, and α_2 are 0.066 V^{-2}, -5.87×10^{4} V and −0.015 V^{-1} (upper plot) and 0.079 V^{-2}, 1.47×10^{-3} V, and −0.0163 V^{-1} (lower plot), respectively. The residual sum of squares for this fit was better at 0.0065 (upper) and 0.0016 (lower). The data is the average of eight dc ramps. (d) Net linear component of the data shown in (c) after subtracting the fit to (3.1) from the experimental data, where open circles and open squares represent data at $2f$ and f, respectively.

to be −0.051 V with (3.1) from the data in Fig. 4(a). This implies that the surface potential of the membrane on the cytoplasmic side is 0.051 V more negative than the surface potential on the extracellular side [Fig. 1]. The value of α calculated with the fit is different at each frequency at 0.126 and 0.089 V^{-2} for the data determined at 781.25 and 390.625 Hz, respectively. Figure 4(b) shows the capacitance-voltage relationship obtained from a second cell. The ψ_s for this cell is more negative with a value of about −0.076 V where a similar value was determined at both frequencies. The value of α is once again different at each frequency being greater at 0.135 V^{-2} for the less noisier higher frequency data compared to 0.108 V^{-2} for the lower frequency data. Shown in Fig. 4(c) is the capacitance-voltage relationship for a third cell. In this case the data was better fit (solid gray line) to a parabolic function with a second term that was linear with voltage. Namely

$$C(\Psi) = C(0)(1 + \alpha(\Psi + \alpha_1)^2 + \alpha_2(\Psi)) \qquad (3.2)$$

where α, α_1, and α_2 are constants. We observed this additional linearity with several cells. We tested if this additional linearity was due to thermal drift by extending the stimulus time before and after the ramp (Fig. 2, inset). We observed that thermal drift if present accounted for about 1 fF. However when there was no thermal drift we still observed the additional linearity in the capacitance-voltage function. Clearly thermal drift cannot explain the discrepancy. A second possibility is that the additional linearity is due to the differential capacitance of the quartz pipette (i.e., quartz not covered by Sylgard) which arises from the change in the voltage dependent capacitance of the double layer at the quartz-saline interface. We tested this by blocking the open end of the pipette with Sylgard and placing it into the external solution. The pipette was subjected to the same voltage signal (Fig. 2, inset dotted line) and the admittance was examined. We found no measurable voltage dependent capacitance associated with the pipette. We conclude that this additional linearity must arise from the cell. To characterize it further we subtract the fit to (3.1) from the experimental data; the data obtained at $2f$ although noisy can be described

by a linear function with a slope and correlation coefficient of -32 fFV^{-1} and -0.71 [Fig. 4(d) circles], respectively. The data at f is very noisy and exhibits a similar slope at -34 fFV^{-1} with much lower correlation coefficient of -0.48 [Fig. 4(d) squares].

We show that the measured capacitance, $\mathrm{Im}(Y)/(2\pi f)$ decreases monotonically as the voltage is ramped from negative to positive voltages [Fig. 2 (lower left)] when the conductance is also voltage dependent [Fig. 2 (upper right)]. In contrast the calculated capacitance [Figs. 3 and 4)] determined with either *algorithm one* or *Barnett's algorithm* exhibits a parabolic shape with voltage at both frequencies. This change arises because R_m is also changing with voltage, and R_s is typically >1 Mohm. The measured capacitance is parabolic with the field when R_m is high (>3 Gohm) and constant with voltage at all frequencies, with the resolution decreasing as R_s increases. When R_m varies with voltage as observed [Fig. 3 (middle panel)] the $\mathrm{Im}(Y)/(2\pi f)$ is parabolic with voltage at f of 781.25 Hz only when R_s is small, for higher R_s the measured capacitance is monotonically decreasing with voltage as observed [Fig. 2 (lower left)]. As the frequency is decreased from $2f$ the parabolic function is apparent at higher R_s up to 5 Mohm, but the signal to noise ratio significantly decreases, presumably because of pink noise (data not shown, [15]). When R_m is voltage dependent but much smaller (5 to 6 fold less) the signal to noise ratio decreases significantly making it difficult to discern the function. Because of the voltage dependent conductance and the typical R_s (4–8 Mohm) obtained in the experiments only cells with high R_m (at least 2 Gohm at the extreme voltages and higher in the middle range) exhibited sufficient signal to noise ratio and were analyzed further. About 10% of the total cells patched ($\approx$150) met this criteria.

To compare the data obtained from different cells, $C(\Psi)$ was normalized to that measured at 0 V, $C(0)$ and plotted against Ψ. The normalized capacitance-voltage plot is shown in Fig. 5(a). There is reasonable agreement among cells with the % change in capacitance ranging from about 0.5% to 0.8% at negative potentials to 0.2% at positive potentials. The solid black line is a fit of data obtained from 5 cells to (3.1) with α at $0.120(\pm 0.010)$ V^{-2} and ψ_s at $-0.073(\pm 0.017)$ V. The same data is plot on a linear scale in Fig. 5(b). There is a reasonable linear relationship between the relative change in the capacitance and the square of the voltage with the slope and correlation coefficient at 0.126 V^{-2} and 0.936, respectively. The model does intercept the ordinate close to zero at -0.0001. Outlined in Fig. 5(c) are capacitance versus voltage plots that were better fit to (3.2) (solid gray line); fit was determined from data obtained from ten (10) cells. To characterize this additional linearity we subtract the fit to (3.1) obtained for each cell from the experimental data and plot the remaining average function in Fig. 5(d). The plot is best fit with a cubic function although within -0.09 and 0.11 V can be described by linear function with slope, intercept and correlation coefficient of -46 fFV^{-1}, 0.002 fF, and 0.98, respectively. On one occasion we observed a sharp peak in the capacitance at -0.045 V with magnitude of 12 fF [inset Fig. 5(d) open triangles]. The fit to the parabolic function in this case was very poor with deviations of up to 40 fF.

Typical current density versus voltage curves are shown in Fig. 5(e). Most cells exhibit a reversal potential of about -0.029 V with a current density at -0.1 and 0.1 V of -1.3 and 4.3 pApF^{-1}, respectively. The plot is fairly linear within -0.08–0.08 V and exhibits a conductance of 20 pSpF^{-1}. We also observed a second current versus voltage curve that was not linear over the entire voltage range and exhibited a reversal potential of -85 mV [Fig. 5(e), circles]. In these cells the current density at -0.1 and 0.1 V is much less at -0.2 and 0.9 pApF^{-1}, respectively. The conductance calculated from the data is 12.7 pSpF^{-1} at negative potentials (-0.12 to -0.07 V) and decreases to 3.36 pSpF^{-1} as the potential becomes more positive (-0.06–0.06). The current density is 10–40 times less than the peak current density of 41 pApF^{-1} measured at 0.1 V in solutions that do not contain channel blockers [17]. In all cases the capacitance-voltage relationships were the same when the reversal potential was at -0.029 and -85 mV [Figs. 5(a) and 5(c)]. HEK cells exhibit various types of voltage dependent potassium [18] and chloride [17] channels. The increased current density at positive potentials is probably due to voltage dependent chloride currents [17] which were not normally blocked in our experiments.

C. Salicylate moves the minimum of the capacitance-voltage function towards zero volts

Salicylate, is one of the few chemicals known to significantly reduce electromechanical coupling in outer hair cells [19]. To establish if salicylate affects the electromechanical coupling in HEK cells we repeated our experiments (Fig. 2, inset) after replacing the extracellular medium with one that contained 10 mM salicylate. We found the admittance-voltage relationships were similar to those shown in Fig. 2. The $\mathrm{Im}(Y_f)/(2\pi f)$ and $\mathrm{Im}(Y_{2f})/(4\pi f)$ decrease monotonically as the voltage extends from negative (hyperpolarizing) to positive (depolarizing) values. $\mathrm{Re}(Y_f)$ and $\mathrm{Re}(Y_{2f})$ still exhibit a parabolic shape with minimum centered at zero. The cell parameters calculated from the admittance data are shown in Fig. 6. The data obtained from both algorithms are presented. We show them to illustrate that the same trends discussed above in Secs. III A and III B are also found in this data. In the presence of salicylate, C changes less with voltage from 8.46 pF at extreme negative potentials to 8.43 pF at 0 V and back up to 8.46 pF at the extreme positive potentials. The R_m exhibits a similar pattern to that observed in the control solution, it is less at the extreme potentials (up to 2 Gohm) and peaks left of the center (4 Gohm), at about -0.020 V (Fig. 6, center panel). As expected, R_s is constant with voltage at 6.7 ± 0.04 Mohms for this ramp. When the results of several ramps are averaged we find that the capacitance is parabolic with voltage with a minimum close to zero [Fig. 7 (left panel)]. Fitting the data to (3.1) we calculate an α and ψ_s of 0.077 V^{-2} and -0.013 V, respectively. When this same cell was in control solution the α was about the same at 0.069 V^{-2} but the ψ_s was much more negative at -0.073 V. Salicylate decreased ψ_s by 60 mV, which caused the minimum of the capacitance-voltage parabola to move towards the center of the voltage axis.

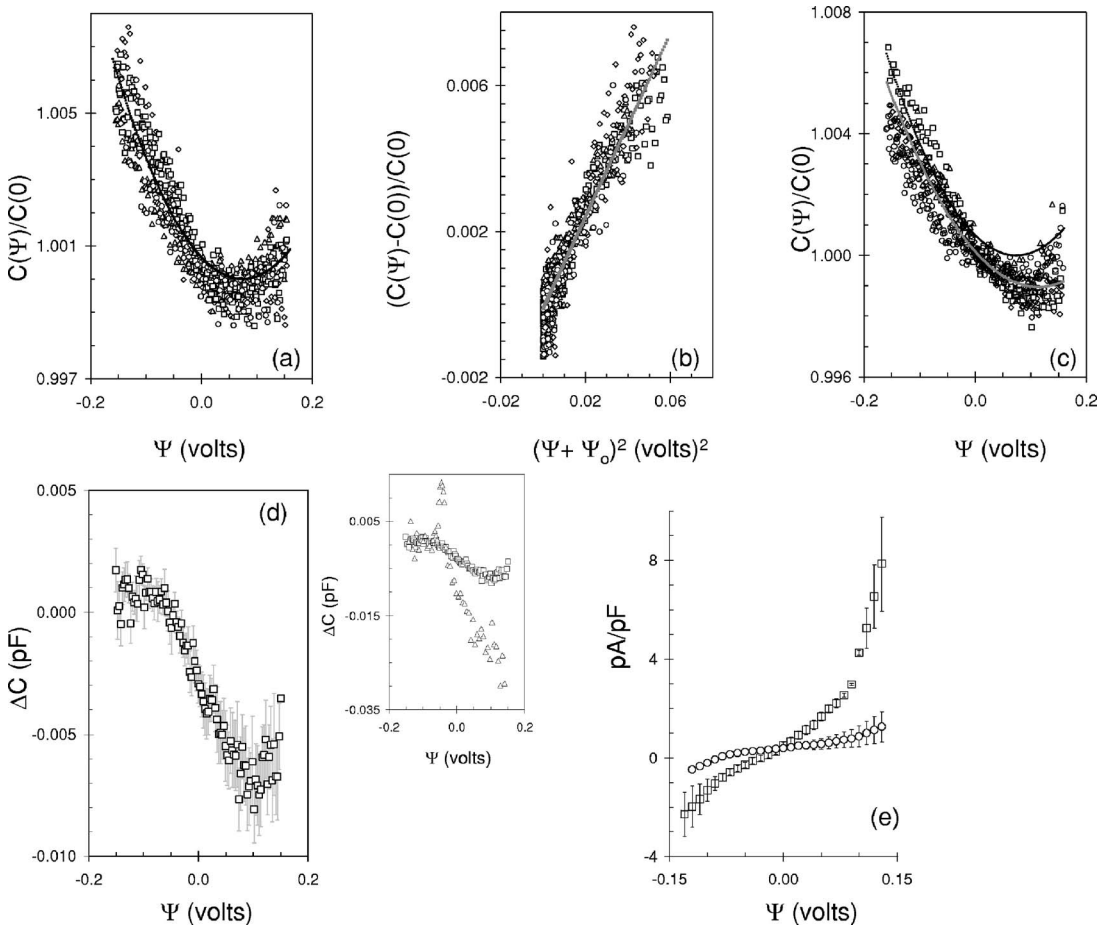

FIG. 5. Membrane capacitance is a function of voltage. (a) Normalized capacitance-voltage plot. The different symbols represent results from 4 different cells. The solid black line is a fit of all data (five cells) to (3.1) where α and ψ_s are 0.120 V^{-2} and −0.073 V. The residual sum of squares is 0.00048. (b) The same data shown in (a) plotted on a linear scale where the solid gray line is a linear fit to all data. (c) Normalized capacitance-voltage plot for four additional cells. The cells ($n=10$) were better fit to (3.2) where α, α_1, and α_2 were found to be 0.0903 V^{-2}, 0.0376 V, and −0.027 V^{-1}, respectively. The residual sum of squares is 0.0007. (d) The nonparabolic component of the data shown in (c) after subtracting the fit to (3.1) from the experimental data. The data (open squares) is the average from 10 cells. The bars represent the standard error of the mean. The inset shows ΔC observed for 1 cell where there is a peak in the capacitance function at −0.045 mV (open triangles). The fit to the parabolic function in this case was poor, the residual sum of squares was 0.02. The nonparabolic component of the data is also shown (open squares). (e) Typical current density versus voltage curves. Open squares: Average current density measured from five cells, the reversal potential is −0.029 V; and open circles: average current density measured from three (3) cells with a reversal potential of −0.085 V. The bars represent standard deviation.

Outlined in Fig. 7(center panel) are the C versus Ψ relationships for three cells where 10 mM sodium salicylate was added to the extracellular solution. $C(\Psi)$ is normalized to that measured at 0 V, $C(0)$. At negative potentials the relative change in the capacitance is less in salicylate at 0.3%–0.5% compared to that observed in normal medium at 0.5%–0.8%. At positive potentials the change is slightly greater in salicylate at 0.2%–0.3% compared to 0.1%–0.2%. The solid black line is a fit of all data (four cells) to (3.1) where α and ψ_s are 0.108(±0.29) V^{-2} and −0.023(±0.009) V, respectively. The same data is plotted on a linear scale in Fig. 7 (right panel). There is a reasonable linear relationship for the change in capacitance against the square of the voltage. The model does traverse the central tendency of this data which is evident by examination of the intercept which is close to zero at 0.00009.

IV. DISCUSSION

A. Unlikely mechanisms for the voltage dependent capacitance

We found that the voltage dependent capacitance (Figs. 3–7) does not originate from the differential capacitance of the double layer at quartz-saline interface and is not due to thermal drift, at most only a few fF result from these processes. Cross-talk between the Re(Y) and Im(Y) components can induce artifacts in the C signal especially when large conductances are observed [20]. We obtained comparable capacitance-voltage plots when we estimated $b(\Psi)$ from the admittance measurements and when we determined $b(\Psi)$ at dc. We also found that the R_m versus voltage plot [Fig. 3(b)] was similar when it was determined at dc and with admittance. As mentioned above in Sec. II D and II E, the only difference was in the absolute value of the estimates; R_m

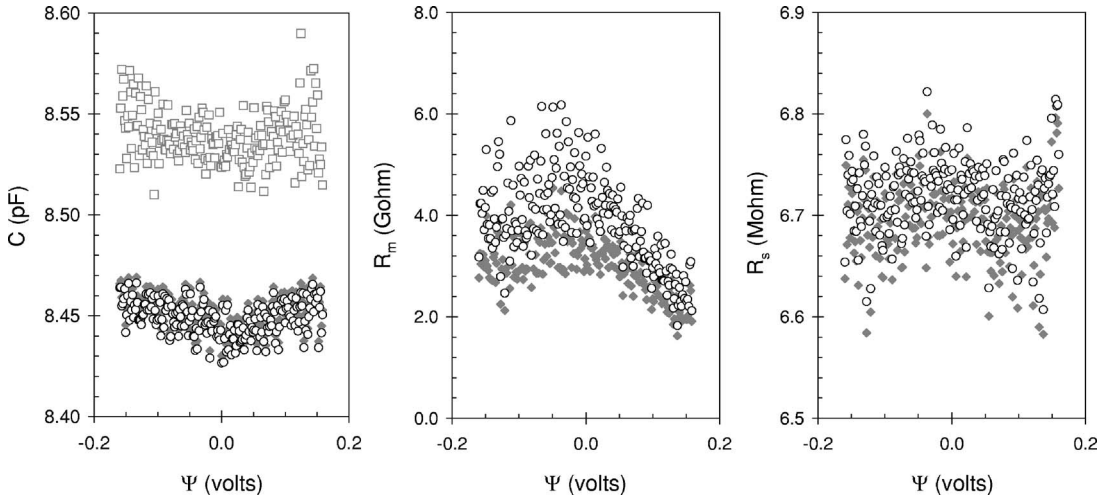

FIG. 6. Cell parameters calculated from admittance obtained during a dc ramp when 10 mM sodium salicylate was added to the external bathing medium and a HEK cell held under whole-cell voltage clamp. The symbols are defined in Fig. 3.

estimated from admittance was less than that at dc when $R_m \geqslant 2$ Gohms (Table I). The signal-to-noise of the capacitance-voltage plot is reduced when the conductance is large especially with increasing R_s. We only analyzed cells that exhibited $R_m \geqslant 2$ Gohms at extreme voltages with even higher values in the middle voltage range. We did this to minimize the influence of voltage dependent currents on the C trace. We achieved low conductances by addition of channel blockers to the solutions.

HEK cells express endogenous voltage-gated (Kv) potassium channels [18]. Tetraethyl ammonium chloride and CsCl block these K currents [18], and both were always added to the extracellular and intracellular solutions in our experiments. In some experiments 1 mM $BaCl_2$ was added to the external solution as an additional block of K currents. We observed the same voltage-dependent capacitance plots (Figs. 3–5) in the presence and absence of $BaCl_2$. Endogenous voltage dependent calcium channels that are sensitive to $NiCl_2$ are present in HEK cells [21]. In experiments when 100 μM $NiCl_2$ was added to the external solution the same capacitance-voltage relationship (Figs. 3–5) was observed. Two voltage-gated chloride conductances are expressed in HEK cells [17] one of them is sensitive to DIDS [17]. We did not usually block the voltage gated chloride channels, but we did conduct several experiments where we added DIDS (130 μM) to the external solution, although we observed a twofold decrease in the conductance similar to that reported [17] we observed similar capacitance-voltage plots. Of the known voltage activated channels we did not block the 350 pS chloride current [17]. It is unlikely that the flux

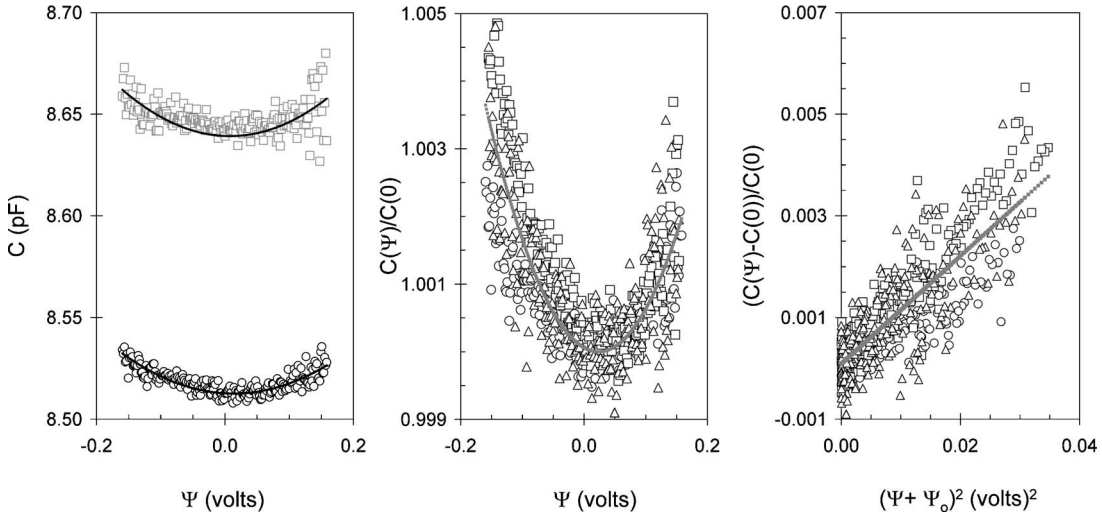

FIG. 7. Capacitance-voltage relationship for HEK cell when 10 mM sodium salicylate was added to external bathing medium. (a) The symbols are defined in Fig. 3. The data is the average of six dc ramps. The solid black lines are fits of the data to (3.1) where α and ψ_s are 0.094 V^{-2} and −0.008 V (upper plot) and 0.077 V^{-2} and −0.013 V (lower plot), respectively. (b) Normalized capacitance voltage plot. The different symbols represent different cells. The solid gray line is a fit of all data (four cells) to (3.1) where α and ψ_s are 0.108 V^{-2} and −0.023 V. The residual sum of squares is 0.00026. (c) The same data shown in (b) plotted on a linear scale where the solid gray line is a linear fit to the data with the slope and correlation coefficient at 0.106 V^{-2} and 0.834, respectively.

through this voltage dependent channel is affecting the gross nature of the capacitance-voltage plot. Voltage-dependent currents influence capacitance signals when the kinetic rate constants of the channels are similar to the angular frequency of the sine wave [20]. If the conductance through this channel was affecting the capacitance-voltage plot the function observed at 4900 and 2450 s^{-1} should be different. This is not the case (Figs. 3, 4, and 6). All this evidence suggests that we measured voltage dependent membrane capacitance in HEK cells and that this does not originate from the flux through voltage dependent channels.

Exocytosis results in a change in the membrane capacitance as a result of incorporation of membrane bound vesicles to the cell membrane and endocytosis causes a decrease in the membrane area and hence capacitance due to internalization or retrieval of vesicles from the cell membrane. It is very unlikely that the capacitance-voltage relationships (Figs. 3–7) are due to regulated or constitutive exocytosis/endocytosis (where regulation implies governed by a secretory event). The reasons are: (i) Voltage dependent calcium channels were blocked by $CoCl_2$ and sometimes also by $NiCl_2$; (ii) release of calcium from calcium stores would be buffered by EGTA; (iii) capacitance-voltage signal was the same upon repetitive ramping of the cell; the signal should vary as all vesicles should not either fuse or be retrieved, simultaneously; (iv) capacitance-voltage plots are not expected to be similar when the holding potential is ramped in either direction (Fig. 2, inset), (v) retrieval or loss of vesicles is not expected to be a function of the cell size [Fig. 5(a) and 5(c)], unless the cell was always incorporating and retrieving the same % of membrane.

Voltage dependent capacitance changes can also originate from redistribution of charges associated with channel proteins within the membrane, well documented is the gating currents of sodium channels [22]. HEK cells express voltage dependent sodium channels that exhibit fast activation and inactivation kinetics and are sensitive to tetrodotoxin [23]. The dc voltage in our experiments was ramped at 0.3 Vs^{-1} (Fig. 2 inset) which would inactivate the channels. However, the region of overlap between the inactivation and activation of the channels lies between −0.05 and 0.01 V [23]. In this region there is a small probability that sodium channel gating currents could be detected. On one occasion we observed a small transient (12 fF) that peaked at −0.045 V [Fig. 5(d) inset]. We suggest that this transient arises from the gating current of sodium channels. Given the above arguments we thus suggest that electromechanical coupling, either by Maxwell stress or electrostriction, is responsible for the voltage-dependent capacitance observed in HEK cells. We make this suggestion because $C(\Psi)$ grows with the square of the voltage (Figs. 4, 5, and 7); capacitance changes are small ($<1\%$) and addition of salicylate moved the minimum of the parabola close to zero volts.

B. Maxwell stress and electrostrictive effects likely origins of the voltage dependent capacitance

Maxwell stress effect originates when there is a change in the electric field within the membrane as the result of a strain; the strain compresses the membrane because of the Coulombic attraction between mobile charges across the membrane. The electrostrictive effect arises because of strain induced change in the dielectric properties of the membrane. This force can cause contraction or expansion depending upon the sign of the electrostriction coefficient. For linear dielectrics both effects cause stresses and strains that are quadratic with the field, E and both are described for ceramics and polymeric materials [24–27]. Electrostrictive effects were demonstrated in dry purple membranes of *Halobacterium salinarium* at fields between 10^6 and 10^8 Vm^{-1} where the membranes thinned during application of an electric field [28]. When the films were orientated (not centric) the minimum of the parabolic function was at positive potentials, when the films were symmetric or weakly orientated the minimum of the parabolic function moved towards zero volts. In this case the films also exhibit direct and converse piezoelectric effects. In HEK cells the minimum of the capacitance-voltage plot is at a positive voltage at about 0.073(±0.017) V implying that the difference between the inner and outer surface potentials is −0.073(±0.017) V and the membrane is asymmetric. Addition of salicylate to the external medium reduces the ψ_s to about −0.023(±0.009) V. This suggests that salicylate adsorbs into the membrane decreasing the intrinsic charge asymmetry of the membrane. This is reasonable as there is much evidence to show that salicylate adsorbs into surfactant [29] and lipid [30–32] assemblies and cell membranes [33] increasing the surface charge density of the membranes, i.e., making it more negative. Its solubility is enhanced, relative to other benzoates, because the carbonyl and hydroxy group can form an intramolecular hydrogen bond [31] which increases its hydrophobic character and helps to drive its penetration into the membrane. Indeed, recent molecular dynamics simulations of a lipid bilayer shows that salicylate penetrates more deeply than chloride, displacing it from the water-bilayer interface [32]. This reduction in the charge asymmetry of the membrane by adsorption of salicylate was also suggested in an atomic force microscopy (AFM) study of the HEK cell [34].

In about 60% of our experiments we also observed an additional linear component in the capacitance-voltage relationship, a differential capacitance of about −46 fFV^{-1} was observed between −0.09 and 0.1 V [Figs. 4(d), 5(c), and 5(d)]. The contribution of charge from this linear component over this voltage region is about 5.7×10^4 electrons, which is greater than the total charge originating from parabolic component (2.4×10^4 electrons), assuming a 10 pF cell. For cells (<20 pF) the charge contribution of the linear component dominates if present. This additional linear component was not observed when salicylate (10 mM) was added to the external medium (Fig. 7) suggesting that significant membrane asymmetry may be necessary to observe it. If this is the case it may also originate from additional electromechanical coupling effect, e.g., piezoelectric effect. The reason that both components were sometimes observed may arise from the nature of the ac stimulus used in the experiments. The stimulus was the sum of two sine waves, one at fundamental frequency, f the second at $2f$, because the response at $2f$ also

contains the response at the second harmonic of the fundamental f this may contribute to detecting a mixture of both electromechanical responses. Repeating the experiments with a sinusoid at one frequency and examining the response of the first and second harmonic independently would enable the separation of the strains that grow quadratically with the field (electrostrictive and Maxwell stress) and strains that are linear (piezoelectric effects) with the field [35], if both are indeed acting in the asymmetric membranes. Finally, there is a possibility that this additional differential capacitance arose from charge distribution in K and Ca channel proteins that occurred during transitions between conformational states (i.e., gating charges), these transitions may occur even though the channels are blocked. This is the explanation suggested to explain the voltage dependent capacitance observed in rat pituitary nerve terminals in the absence of sodium channels [36] in this case the voltage capacitance function was similar to that shown in Fig. 5(d) where the capacitance decreased as the holding potential became more positive decreasing by up to 61 fF at 0.05 V.

Cell membrane capacitance is the sum of the capacitance of its individual components added in series, namely hydrophobic chains, the hydrophilic component including cytoskeleton and the capacitance of the double layer in the surrounding cytoplasmic and extracellular compartments. Because the capacitance of the hydrophobic core is small it dominates the measurement, which is the same for lipid bilayers when the capacitance is measured in solutions at biological ionic strengths (>0.1 M [9]). This implies that the proportionality constant α should represent a mechanical characteristic of the hydrophobic core of the membrane and not that of cytoskeleton. Indeed, analysis shows at least for smectic bilayers that the magnitude of α represents the membrane's ability to compress and bend in response to a voltage [16]. Their theoretical analysis is in reasonable agreement with α determined experimentally for bilayer lipid membrane (BLM) at $0.018(\pm 0.002)$ V^{-2} [9]. The α determined for HEK cell membrane is about six (6) times greater at $0.12(\pm 0.01)$ to $0.108(\pm 0.29)$ V^{-2} and much noisier than values determined for BLMs. The reason for the increased noise is the residual ion channel flux, which is in agreement with observations made with BLMs [37]. Both channel activity and capacitance changes were observed in BLMs that contained a few gramicidin channels. They found that the noise on both α and ψ_s grew worse as they increased the number of channels [37]. We found that the signal to noise ratio deteriorates with cells that exhibit high conductances; indeed our signal to noise ratio is much worse than that measured with BLMs because of the residual flux.

A second reason for the discrepancy in α is a difference in membrane tension. BLMs exhibit tension of $2-10$ mNm^{-1}, cell membranes have extensive number of folds [38] and generally exhibit low surface tensions 10^{-5} Nm^{-1} [39]. Theoretical analysis suggest that α should be larger by about 40% if surface undulations are present at tensions of 2 mNm^{-1} [16]. Because the plasma membrane exhibits tensions 50–100 times less than this, cell membrane folds or surface undulations are expected to have a greater impact increasing the value of α. Indirect evidence to support this is reported [38]. Specifically, when cells were inflated by application of a hydrostatic pressure, C was observed to increase as the cell membrane was unfolding, increase in C was observed when pressure was applied, it was not just observed when all folds in the membrane had flattened. In this case total C change associated with membrane unfolding and thinning was found to be about 77 fF for a fully inflated cell of initial capacitance 4 pF [38], this is about 2% change in capacitance. We measure a smaller capacitance change up to 0.8% (Fig. 5) in the presence of an electric field suggesting that we did not reach the maximum C change.

Third reason for the discrepancy in α is the difference in composition. The plasma membrane is a multicomponent mixture of lipids and proteins arranged asymmetrically, while the BLM examined [9] was a bilayer composed of two components: A monolayer of phosphatidylserine and a monolayer of phosphatidylethanolamine. In the former many different proteins and lipids may respond to the field, in the latter only two different lipids respond to the field. In addition, biological membranes of cells exhibit domains. For example, cholesterol in cell membranes is associated with phospholipids in the bilayer, and lipid and protein stabilized domains coined rafts and caveolae, respectively. Although, there is no evidence that HEK cells exhibit the membrane pits indicative of caveolae [40], it is possible that the field could cause a redistribution of proteins or some other component(s) among domains which in turn would alter the capacitance. To address this it is instructive to examine the earlier results on BLMs made from solvents [41]. In this case the voltage dependent capacitance is described by the same function (3.1) with values for α that are at least 15 fold greater than that observed for HEK cell membrane at $2-10$ V^{-2}. Although, compression and bending of the BLM was reported, the proposed mechanism for the significant voltage dependent capacitance was the flux of solvent from the BLM to the reservoir (i.e., the annulus of bulk lipid suspension surrounding the BLM and the microlenses of solvent within the BLM) [42]. In the plasma membrane it is likely that the application of an electric field changes the chemical potential of the components causing lateral fluxes among different domains. If this flux occurred at times $\ll 1$ second and contributed to the voltage dependent capacitance function then this would increase α and make the membrane appear to be softer.

We find it useful later for Secs. IV C and IV D to have an estimate of mechanical constants of HEK membrane from the strain induced by the electric field, E. Because the theory describing the effects of E on plasma membranes that exhibit surface undulations or folds is not developed we estimate membrane stiffness, K and Young's modulus, Z assuming E acts on a flat membrane (Supplementary material). We also assume that any lateral flux of components among domains in the membrane does not contribute to α. This may be invalid if the cell membrane behaves like a solvent containing BLM (see above). Specifically, for a flat membrane that exhibits no undulations and where there is no flux among domains the change of C can be written as

$$\frac{\Delta C}{C} = \frac{\epsilon_o \epsilon_m E^2}{Z}\left[1 - \frac{3a_1}{2\epsilon_m} + \frac{a_1^2}{2\epsilon_m^2}\right] \tag{4.1}$$

where ϵ_m is the relative dielectric constant of the undeformed membrane, ϵ_o is the relative permittivity of free space and a_1

is the change in the relative permittivity with change in shape at constant volume. Assuming the electrostrictive effect is negligible, $a_1 \ll \epsilon_m$ then

$$\frac{\Delta C}{C} \approx \frac{1}{Z}\epsilon_o \epsilon_m E^2 \approx \frac{C_m}{Zd}\psi_t^2.$$

Making use of (2.2) and (2.3) then

$$\frac{C(\Psi) - C(0)}{C(0)} \approx \frac{C_m}{K}(\Psi + \psi_s)^2 \tag{4.2}$$

where C_m is the specific capacitance of the membrane. Comparing with (3.1) $\alpha \equiv C_m/K$. We assume C_m is 0.5 μFcm^{-2} and estimate K at 42 ($\pm$3) mNm^{-1} in solutions that contain K and Ca blockers (Fig. 5) and 53 ($\pm$15) mNm^{-1} in salicylate (Fig. 7).

A stiffness of 40–70 mNm^{-1} is comparable to the K obtained for vesicles made from the brush-border membranes of the eel intestine at 87 mNm^{-1} [43] and the vesicles made from brush border membranes of the rat at between 50 and 150 mNm^{-1} [44]. It is much less than the best estimate for membranes of red blood cells (RBCs) at 500 mNm^{-1} [45,46]. It is also 5 to 6 times less than the best estimates for the elastic area compressibility modulus for membranes made from fluid phase phosphatidylcholine bilayers [47]. They found that K was fairly constant with an average value of 243 mNm^{-1} for diacyl phosphatidylcholine bilayers with long (C-22) and short chains (C-12) and various number (0 to 6) of carbon double bonds. Given the approximations we use to estimate K and Z, these differences are to be expected. Better estimates of K for HEK cell membrane could be obtained by controlling membrane tension and minimizing undulations by lowering temperature. This should be done in conjunction with development of theory to analyze folded plasma membranes. We note that some of the earlier estimates of K for model bilayer systems also underestimated K as thermal undulations were not adequately considered (see discussion in [47]).

C. Comparison with experimental measurements obtained with AFM

We calculate Young's modulus, Z of about 1×10^7 Nm^{-2} for the HEK membrane. This value is much greater (about 10^3 times) than that estimated with AFM at 5000 to 7500 Nm^{-2} for HEK cells [34] and for other cultured mammalian cells at 10^4 and 10^3 Nm^{-2} [48,49]. Clearly both the capacitance and AFM measurements are estimating different elastic parameters of the cell membrane. As mentioned the voltage dependent capacitance measurements (Figs. 5 and 7) reveal the elasticity of the inner hydrophobic part of the membrane whereas the softer cytoskeleton is sensed by AFM [50]. The techniques differ in another way. For the capacitance measurements we electrically stimulate in whole-cell mode and measure the average change in the capacitance of all the membrane. This is a global stimulation and response. For the force microscopy techniques [48,49] the probe makes a local indentation and the forces are measured locally. In the AFM study of HEK cells a slightly different approach was used; a cell was stimulated in whole-cell voltage clamp and the response was measured locally from the deflection of the cantilever that was positioned normal to the cell surface. In this way, small displacements ($\Delta z \approx 10^{-10}$ m) and forces ($\Delta F \approx 0.01$ nN) were detected upon changing the holding potential of a HEK cell immersed in normal high concentrations of cytoplasmic K and normal high concentrations of extracellular Na [34]. When the cell was hyperpolarized ($\Psi < -0.06$ V) the cantilever moved towards the cell as the force became more attractive. The force became more repulsive (the cantilever moved away from the cell) when the cell was depolarized ($\Psi > -0.06$ V). The force was linear with Ψ between the potentials -0.18 to $+0.04$ V. Addition of salicylate minimized these displacements to the level of the baseline noise. From their observations and model they proposed that this voltage dependent movement originates from a change in surface tension, $\Delta\gamma$ of the membrane which was reduced in the presence of salicylate. They suggested that salicylate reduced this tension by adsorbing onto the outer leaflet increasing its negative charge, thereby reducing the charge difference between the leaflets. We show in agreement with their observation that salicylate adsorbs into the HEK membrane decreasing the charge asymmetry (Fig. 7), but we also show that this does not work by reducing the membrane tension as they proposed. We do this by deriving a new expression for the voltage dependent tension that is similar to one reported [51], but different from that in [34].

Gibb's adsorption equation for a planar membrane is

$$q_p = -\frac{d\gamma}{d\Psi}_{(T,\mu,P,e)} \tag{4.3}$$

where (μ) is the chemical potential of the immobile components (lipids and proteins), that make up the membrane, T: Temperature, P: Hydrostatic pressure, and e: Extension ratio within the plane of membrane (see Supplementary material). The holding potential, Ψ is the only measurable parameter in (4.3) the polarization charge density, q_p and membrane tension, γ are unknown. We estimate q_p with $q_p = C_m\psi_t$ by assuming the specific capacitance, C_m of the membrane is constant with voltage. We derive an expression for the potential difference across a flat membrane, ψ_t with the Gouy-Chapman-Grahame theory [52,53] (see Supplementary Material). Where we apply the additional assumptions that there are no free charges within the membrane, the gradient of the potential is constant within the membrane and the ionic strength is the same in each compartment and is dominated by a 1:1 electrolyte of concentration, c [54]. q_p is then given by:

$$q_p = \frac{C_m \kappa \epsilon \epsilon_o}{\kappa \epsilon \epsilon_o + 2C_m}\left[\Psi + \frac{2RT}{F}\,\mathrm{a\,sinh}\left(\frac{(\sigma_i^o + \sigma_e^o)F}{2\kappa\epsilon\epsilon_o RT}\right) - \frac{2\sigma_e^o}{\epsilon\epsilon_o\kappa}\right] \tag{4.4}$$

where κ is the reciprocal Debye length and defined for a 1:1 electrolyte as

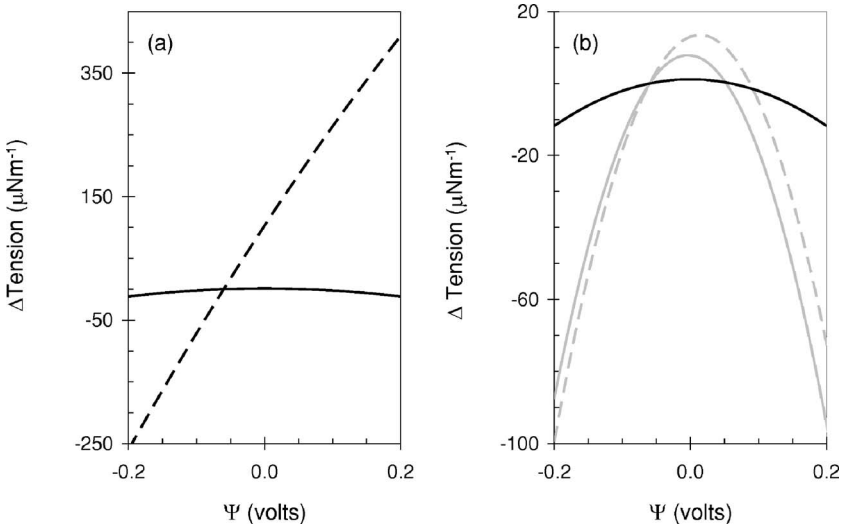

FIG. 8. Tension change as a function of Ψ calculated with expression in [34] [black lines, (a) and (b)] and expression (4.6) [gray lines, (b)]. The dashed black and gray lines represents $\Delta\gamma$ calculated with $\sigma_i^o \equiv -0.018$ cm^{-2} and $\sigma_e^o \equiv -0.005$ cm^{-2}. The solid black and gray lines represent $\Delta\gamma$ calculated with $\sigma_i^o \equiv \sigma_e^o \equiv -0.018$ cm^{-2}. The other parameters were C_m: 0.005 Fm^{-2}, $c_i \equiv c_e \equiv 0.14$ M, Ψ_r: -0.060 V, ϵ: 80.4 and T: 20 °C.

$$\kappa^2 = F^2\left[\frac{2c}{\epsilon_o \epsilon RT}\right], \tag{4.5}$$

σ_i^o and σ_e^o are the surface charge density of the internal and external leaflets; ϵ is the relative permittivity of the solution, R and F are gas and Faraday constants. Substituting (4.4) into (4.3) and integrating from a reference holding potential, Ψ_r to Ψ we find

$$\Delta\gamma = -\frac{C_m \epsilon\epsilon_o \kappa}{\epsilon\epsilon_o\kappa + 2C_m}\left[\frac{1}{2}(\Psi^2 - \Psi_r^2) + \left[\frac{2RT}{F}\text{a sinh}\left(\frac{(\sigma_i^o + \sigma_e^o)F}{2\kappa\epsilon\epsilon_o RT}\right) - \frac{2\sigma_e^o}{\epsilon\epsilon_o\kappa}\right](\Psi - \Psi_r)\right], \tag{4.6}$$

where $\Delta\gamma = \gamma(\Psi) - \gamma(\Psi_r)$. We also re-derive the expression in [34] (Supplementary material). We compare the results calculated from both expressions in Fig. 8.

When the surface charge density of each leaflet is different, $\Delta\gamma$ determined with the expression of Zhang *et al.*, is pseudo-linear with Ψ, at least within the biological range, where $\Delta\gamma$ is -71 and 264 μNm^{-1} at -0.1 and 0.1 V, respectively. The voltage where the tension is maximum is at a very positive potential of 1.3 V. When the surface charge density is the same on each leaflet $\Delta\gamma$ is significantly less at -2 μNm^{-1} at both -0.1 and 0.1 V. The voltage when the tension is maximum is now at zero volts [Fig. 8]. This contrasts $\Delta\gamma$ determined with (4.6) [Fig. 8(b)]. When the surface charge density on each leaflet is different the maximum is at 0.016 V with a $\Delta\gamma$ of -18 and -7 μNm^{-1} at -0.1 and 0.1 V, respectively. When the surface charge density is identical on both leaflets the maximum is once again at zero volts but there is not a significant change in $\Delta\gamma$, values of -15 and -20 μNm^{-1} are calculated for -0.1 and 0.1 V, respectively. Their model suggests that $\Delta\gamma$ should be almost linear with Ψ at voltages applicable to biology and should be reduced significantly upon equalizing the surface charge density on each leaflet. This calculation seemed to resemble their experimental observations; displacements were linear with voltage and disappeared upon addition of salicylate. Their calculated significant reduction in $\Delta\gamma$ led them to conclude that salicylate reduced the intramembrane electric field which in turn reduced the movement. On the contrary, calculations with (4.6) show as published earlier [51] that significant voltage dependent tension can occur when the surface charge density of both leaflets is the same [Fig. 8(b)]. The reason for this discrepancy is that the boundary conditions, used to integrate the Lippmann equation [52,53] were inappropriate and approximation $\psi_t \equiv \Psi$ [see Fig. 1] invalid (see Supplementary Material). Specifically, we show within the assumptions of the tension hypothesis, that if small electrically evoked displacements are detected by the AFM when there is a different charge on each leaflet, they should also be measurable when the surface charge density on both leaflets is identical. In addition, it suggests that the tension should be parabolic with voltage, this was not observed although it may be that the maximum is at a more positive potential than probed experimentally. Experiments with the axon of the giant squid show that intracellular pressure was proportional to the square of the voltage [55] and exhibited a maximum at 0.061 V [51]. In this case membrane thinning or voltage dependent tension changes [51] were suggested to be probable origins of pressure changes. These pressure results can be explained in terms of voltage dependent tension changes despite the gross assumptions inherent in Gouy-Chapman-Grahame theory [52,53]. Although, voltage dependent tension effects may be part of the origin of the force, because they [34] did not show that displacements were parabolic with the voltage it raises doubt whether this hypothesis is correct, at least as derived from (4.3) together with the assumed resultant action of the forces on the AFM cantilever. At present, both cannot explain the results in salicylate. However, we do agree that salicylate makes the membrane more symmetric (Fig. 7), perhaps the salicylate effect measured with the AFM results form this observation; a more centric or less orientated material will have a different response to that observed from an acentric or asymmetric membrane [28]. We found that the additional linear component [Figs. 5(c) and 5(d)] was absent or disappeared into the noise floor when salicylate was added to the external solution (Fig. 7), perhaps this linear component is the origin of the force in the AFM experiments.

D. Estimation of the force produced in response to the electrical field in membranes and cells

We show that the change in the capacitance of the HEK cell membrane is up to 0.8% at field strengths up to 5×10^7 Vm^{-1} (Figs. 5 and 7). From the measured change in C (0.1%–0.8%) and calculated K (50 mNm^{-1}) we estimate a range of Δd of 0.003 to 0.025 nm (d=3 nm) and range for ΔF of 0.15–1.25 pN. (Note, because we do not estimate the force acting during the linear component this is probably an underestimate). This is within the range measured for the force acting on a membrane tether pulled from a HEK cell that was also whole-cell voltage clamped; a total force of 1 to 2 pN over the physiological region is calculated [56]. The lower range of the force is also similar to that observed when a Chinese hamster ovary cell, CHO, was placed in a microchamber and electrically stimulated by an ac field (10 mV peak to peak at frequencies from 0.2 to 4 KHz), a force of 0.3 pN was measured throughout the frequency range [8]. We have observed similar capacitance-voltage relationships with CHO cells as observed with HEK cells [i.e., Figs. 5 and 7], this together with the magnitude of the experimental force [8] suggests that both may originate either from compression or bending as discussed in this work and/or by voltage-dependent tension effects [34,57]. However, if this is the case a component of the measured force [56] should exhibit a parabolic dependence with the field which was not reported, although it may be convoluted in the linear relationship [56].

Estimates from *in vitro* experiments on single OHCs show that the force ranges from 30 [2] to 100 $pNmV^{-1}$ [4], or up to 2 nN from stiffness measurements (displacement 0.2 μm stiffness 8.5 mNm^{-1}, [5]). Recent indirect estimates from measurements of the intra-cochlear pressure suggest that the active force produced by an OHC *in vivo* is about 660 pN [6]. These estimates are much greater than force measurements on membrane tethers pulled from OHCs that were whole-cell voltage clamped. This force produced is about 0.3 $pNmV^{-1}$ with total force acting over the voltage region of about 60 pN. The discrepancies may arise from the different components of the cell probed and geometry of the experimental system (cylindrical membrane tether [56] versus whole-cell axial force [5]). These force discrepancies have still to be explained (60 versus 1000 pN) but are clearly much greater than the estimates found for the HEK cell membrane at 1 to 2 pN.

E. Implications of results to mammalian cells transfected with prestin and outer hair cells

The membrane of the outer hair cell increases its capacitance by up to 90% upon application of a field [58]. This voltage-dependent capacitance function is bell-shaped and exhibits asymmetry [59]. The capacitance-voltage signal is the convolution of at least two interdependent functions; the well-known symmetric gaussian (half-width $\approx$0.1 V) and less well-documented non-gaussian function. For an OHC the total number of charges originating from both components is $\approx 18 \times 10^6$ electrons. When HEK cells are transfected with prestin, the capacitance-voltage signal is also a convolution of at least two functions, but the total charge varies from cell to cell, and is at most 30% (5×10^6 electrons) of that observed in OHCs. This is generally greater than measured from gating charges of sodium channels in neurons at about 6×10^4 electrons [36]. It is also generally much greater than that measured for HEK cells where the charge from the parabolic and linear components is about the same at 5×10^4 electrons (Fig. 5, assuming a 20 pF cell). The enormity of the charge measured with OHCs and prestin-transfected cells is only approached by addition of hydrophobic ions to membranes which also induces a bell-shaped function [60] and measurements made with BLMs in wet solvents [41] in the latter case the capacitance is parabolic with the field and is probably dominated by solvent-induced Maxwell-stress mechanisms [42].

We can conclude from our results with mammalian cells, and from the reported observations with sodium channels in neurons [22,36] that the charge contributions from the collective response of membrane proteins (e.g., transporters, channels, and pumps) and lipids in the field is minimal relative to that observed with prestin in the membrane. The enormity of charge may result from chloride movement within prestin [61]. In comparison to HEK membranes, OHC membranes do not behave as linear dielectrics. Indeed, OHCs exhibit a piezoelectric effect both the converse effect (electrical stress causing polarization and strain) and direct effect (mechanical stress producing strain and polarization) were experimentally measured on isolated OHCs [62]. The origin of this effect is unknown. It is possible that in OHCs the effect could originate from electrostriction as it does for ferroelectrics [26] in this way the piezoelectric coefficient would depend upon the induced polarization and could be controlled by the field. This would provide an explanation for the nonlinearity of the cell's response, as it allows the cell to optimize its sensitivity (i.e., tune itself) to the field.

V. CONCLUSIONS

1. The voltage dependent capacitance of HEK cell membrane grows with the square of the potential. Fitting the data to (3.1) revealed a minimum of 0.073(±0.017) V and a proportionality constant of 0.120(±0.009) V^{-2} in solutions that contain Ca and K channel blockers.

2. Addition of salicylate to the external medium did not change the rate at which the capacitance grows with voltage, but it did move the minimum to a more negative potential of 0.023 (±0.009) V. We suggest that salicylate adsorbs to the external leaflet decreasing the natural charge asymmetry of the membrane.

3. We also observed an additional linear component in the capacitance-voltage relationship in cells submerged in blocking solutions, but not when 10 mM salicylate was added to the external medium. The capacitance decreased by about −46 fF V^{-1} from −0.09 to 0.1 V. We suggest that this component may arise either from an additional electromechanical effect (e.g., a piezoelectric effect) or alternatively it may arise from charge distribution in channel proteins as they proceed between conformational states.

4. The effective stiffness, K of the membrane was esti-

mated to range between 40 and 50 mNm^{-1}. This was calculated assuming the membrane is flat and deformation is caused only by Maxwell stress effects. From this and the small % change in the capacitance we estimate that the electromechanical force acting is about 0.2–1.3 pN. This is an estimate, as the electrostrictive effect was assumed negligible and thermal undulations or membrane folds were not considered. The electrostrictive effect, if present, could be measured by stimulating the cell with a sinusoidal at one frequency and examining the response at the second harmonic. Undulations could be minimized by conducting experiments at a higher osmotic pressure or lower temperature. In addition, better estimates of K could be made if the noise within the capacitance traces is reduced. We found the estimates of α were more susceptible to noise than estimates of ψ_s. The estimates could be improved by replacing the dual-sinusoidal ac stimulus with a multi-frequency ac stimulus. In this way, measurements of voltage dependent capacitance could be used [9,16] to estimate mechanical properties of cell membranes.

5. We show that the electrically evoked displacements of HEK cells measured with the AFM [34] cannot be explained by the tension hypothesis as derived with Gibb's equation for a flat membrane with the boundary conditions (4.3). Specifically we show that this hypothesis cannot explain their results in salicylate containing solutions when the displacements disappear into the noise floor.

6. The charge movement within the membrane of HEK cells as a result of the field is approximately 2×10^4 electrons (assuming a 10 pF cell) and increases to about 7×10^4 electrons if there is a linear component. This is small relative to that produced in prestin-transfected cells (up to 5×10^6 electrons). This suggests that the charge contributions from the collective response of membrane proteins and lipids in the field is insignificant relative to that observed when prestin is within the membrane.

ACKNOWLEDGMENTS

We thank J. Wooltorton for assisting with the preparation of the patch-pipettes, and for his insights on sodium channels. We thank R.A. Eatock for loan of the setup to cover the patch pipettes with Sylgard. We also thank V. Anjan and R Urginov for technical assistance. We are very grateful to D. Barnett and S. Lempkas for providing their MATLAB program (NWLS) to calculate the electrical parameters of the cell. We are also grateful to N. Baker and Y. Song for comments on the manuscript. Work supported in part by Keck Center for Computational Biology under NLM training Grant No. ITI5LM07093 to BF and NIH Grant No. R01-DC00354 to WEB.

[1] W. E. Brownell, C. R. Bader, D. Bertrand, and Y. de Ribaupierre, Science **227**, 194 (1985).
[2] G. Frank, W. Hemmert, and A. W. Gummer, Proc. Natl. Acad. Sci. U.S.A. **96**, 4420 (1999).
[3] M. C. Liberman, J. Gao, D. Z. Z. He, X. Wu, S. Jia, and J. Zuo, Nature (London) **419**, 300 (2002).
[4] K. H. Iwasa and M. Adachi, Biophys. J. **73**, 546 (1997).
[5] D. Z. Z. He and P. Dallos, Proc. Natl. Acad. Sci. U.S.A. **96**, 8223 (1999).
[6] E. S. Olson, J. Acoust. Soc. Am. **115**, 1230 (2004).
[7] J. Zheng, W. Shen, D. Z. Z. He, K. B. Long, L. D. Madison, and P. Dallos, Nature (London) **405**, 149 (2000).
[8] J. Ludwig, D. Oliver, G. Frank, N. Klöcker, A. W. Gummer, and B. Fakler, Proc. Natl. Acad. Sci. U.S.A. **98**, 4178 (2001).
[9] O. Alvarez and R. Latorre, Biophys. J. **21**, 1 (1978).
[10] J. Santos-Sacchi, S. Kakehata, and S. Takahashi, J. Physiol. (London) **510**, 225 (1998).
[11] D. W. Barnett and S. Misler, Biophys. J. **72**, 1641 (1997).
[12] B. Farrell, R. Ugrinov, and W. E. Brownell, in *Auditory Mechanisms: Processes and Models*, edited by A. Nuttall, P. Gillespie, T. Ren, and K. Grosh (World Scientific, Singapore, 2006) pp. 230–231.
[13] J. A. F. Op den Kamp, Annu. Rev. Biochem. **48**, 47 (1979); P. F. Devaux, Biochemistry **30**, 1163 (1991); P. F. Devaux and R. Morris, Traffic **5**, 241 (2004).
[14] V. Rohlicek and J. Rohlicek, Physiol. Res. **42**, 423 (1993); V. Rohlicek and A. Schmid, Pflügers Arch. **428**, 30 (1994); D. F. Donnelly, Biophys. J. **66**, 873 (1994).
[15] P. Chen and K. D. Gillis, Biophys. J. **79**, 2162 (2000).
[16] M. Partenskii and P. C. Jordan, Mol. Phys. **98**, 193 (2000).
[17] G. Zhu, Y. Zhang, H. Xu, and C. Jiang, J. Neurosci. Methods **81**, 73 (1998).
[18] N. Gamper, S. Fillon, S. M. Huber, Y. Feng, T. Kobayashi, P. Cohen, and F. Lang, Pflügers Arch. **443**, 625 (2002); N. Gamper, S. Fillon, Y. Feng, B. Friedrich, P. A. Lang, G. Henke, S. M. Huber, T. Kobayashi, P. Cohen, and F. Lang, *ibid.* **445**, 60 (2002).
[19] W. E. Shehata, W. E. Brownell, and R. Dieler, Acta Oto-Laryngol. **111**, 707 (1991); M. J. Tunstall, J. E. Gale, and J. F. Ashmore, J. Physiol. (London) **485**, 739 (1995); S. Kakehata and J. Santos-Sacchi, J. Neurosci. **16**, 4881 (1996).
[20] K. S. Cole, *Membranes, Ions and Impulses* (University of California Press, Berkeley, 1972); K. Debus, J. Hartmann, G. Kilic, and M. Lindau, Biophys. J. **69**, 2808 (1995).
[21] S. Berjukow, F. Doring, M. Froschmayr, M. Grabner, H. Glossmann, and S. Hering, Br. J. Pharmacol. **118**, 748 (1996).
[22] C. M. Armstrong and F. Bezanilla, Nature (London) **242**, 459 (1973).
[23] T. R. Cummins, J. Zhou, F. J. Sigworth, C. Ukomadu, M. Stephan, L. J. Ptacek, and W. S. Agnew, Neuron **10**, 667 (1993).
[24] I. Krakovsky, T. Romijn, and A. Posthuma de Boer, J. Appl. Phys. **85**, 628 (1999).
[25] T. Yamwong, A. M. Voice, and G. R. Davies, J. Appl. Phys. **91**, 1472 (2002).
[26] R. E. Newnham, V. Sundar, R. Yimnirun, J. Su, and Q. M. Zhang, J. Phys. Chem. B **101**, 10141 (1997).
[27] W. Lehmann, H. Skupin, C. Tolksdorf, E. Gebhard, R. Zentel,

P. Kruger, M. Losche, and F. Kremer, Nature (London) **410**, 447 (2001).
[28] P. Kietis, M. Vengris, and L. Valkunas, Biophys. J. **80**, 1631 (2001).
[29] Z. Lin, J. J. Cai, L. E. Scriven, and H. T. Davis, J. Phys. Chem. **98**, 5984 (1994).
[30] S. McLaughlin, Nature (London) **243**, 234 (1973).
[31] J. Gutknecht, J. Membr. Biol. **115**, 253 (1990).
[32] Y. Song, V. Guallar, and N. A. Baker, Biochemistry **44**, 13425 (2005).
[33] H. Levitan and J. L. Barker, Science **176**, 1423 (1972); D. Attwell, C. Bergman, and C. Ojeda, J. Physiol. (London) **295**, 69 (1979); I. Cohen, D. Noble, M. Ohba, and C. Ojeda, *ibid.* **297**, 163 (1979).
[34] P.-C. Zhang, A. M. Keleshian, and F. Sachs, Nature (London) **413**, 428 (2001).
[35] W. Carius, J. Colloid Interface Sci. **57**, 301 (1976).
[36] G. Kilic and M. Lindau, Biophys. J. **80**, 1220 (2001).
[37] S. Toyama, A. Nakamura, and F. Toda, Biophys. J. **59**, 939 (1991).
[38] C. Solsona, B. Innocenti, and J. M. Fernandez, Biophys. J. **74**, 1061 (1998).
[39] J. Dai and M. P. Sheetz, Biophys. J. **68**, 988 (1995); R. M. Hochmuth, J.-Y. Shao, J. Dai, and M. P. Sheetz, *ibid.* **70**, 358 (1996).
[40] Y. Wei, X. Yang, Q. Liu, A. Wilkins, and H. A. Chapman, J. Cell Biol. **144**, 1285 (1999); L. Wang, M. A. Connelly, A. G. Ostermeyer, H.-h. Chen, D. L. Williams, and D. A. Brown, J. Lipid Res. **44**, 807 (2003).
[41] S. H. White, Biophys. J. **10**, 1127 (1970); D. Wobschall, J. Colloid Interface Sci. **40**, 417 (1972); R. Benz, O. Frohlich, P. Lauger, and M. Montal, Biochim. Biophys. Acta **394**, 323, (1975); P. Schoch, D. F. Sargent, and R. Schwyzer, J. Membr. Biol. **46**, 71 (1979).
[42] S. H. White, Science **207**, 1075 (1980); S. H. White and W. Chang, Biophys. J. **36**, 449 (1981).
[43] P. Alves, G. Soveral, R. I. Macey, and T. F. Moura, J. Membr. Biol. **171**, 171 (1999).
[44] S. Miyamoto, T. Maeda, and S. Fujime, Biophys. J. **53**, 505 (1988).
[45] C. Katnik and R. Waugh, Biophys. J. **57**, 877 (1990).
[46] D. Needham and R. S. Nunn, Biophys. J. **58**, 997 (1990).
[47] W. Rawicz, K. C. Olbrich, T. McIntosh, D. Needham, and E. Evans, Biophys. J. **79**, 328 (2000).
[48] M. Lekka, P. Laidler, D. Gil, J. Lekki, Z. Stachura, and A. Z. Hrynkiewicz, Eur. Biophys. J. **28**, 312 (1999).
[49] M. Lekka, P. Laidler, J. Ignacak, M. Labedz, J. Lekki, H. Struszczyk, Z. Stachura, and A. Z. Hrynkiewicz., Biochim. Biophys. Acta **1540**, 127 (2001).
[50] M. Radmacher, IEEE Eng. Med. Biol. Mag. **16**, 47 (1997).
[51] V. Malev and A. I. Rusanov, J. Theor. Biol. **136**, 295 (1989).
[52] D. C. Grahame, Chem. Rev. (Washington, D.C.) **41**, 441 (1947).
[53] E. J. W. Verwey and J. TH. G. Overbeek, *Theory of the Stability of Lyophobic Colloids* (Elsevier Press, NY, 1948); J. Lyklema, *Fundamentals of Interface and Colloid Science II: Solid-liquid Interfaces* (Academic Press, London, 1991).
[54] C. T. Everitt and D. A. Haydon, J. Theor. Biol. **18**, 371 (1968); S. Genet, R. Costalat, and J. Burger, Acta Biotheor. **48**, 273 (2000).
[55] S. Terakawa, J. Physiol. (London) **369**, 229 (1985).
[56] B. Anvari, F. Qian, F. A. Pereira, and W. E. Brownell, in *Auditory Mechanisms: Processes and Models*, edited by A. Nuttall, P. Gillespie, T. Ren, and K. Grosh (World Scientific, Singapore, 2006) pp. 268–274.
[57] E. Glassinger, A. C. Lee, and R. M. Raphael, Phys. Rev. E **72**, 041926 (2005).
[58] J. Santos-Sacchi, J. Neurosci. **11**, 3096 (1991).
[59] J. Santos-Sacchi and E. Navarrete, Pflügers Arch. **444**, 99 (2002).
[60] J. M. Fernandez, R. E. Taylor, and F. Bezanilla, J. Gen. Physiol. **82**, 331 (1983).
[61] D. Oliver, D. Z. Z. He, N. Klocker, J. Ludwig, U. Schulute, S. Waldegger, J. P. Ruppersberg, P. Dallos, and B. Fakler, Science **292**, 2340 (2001).
[62] X.-X. Dong, M. Ospeck, and K. H. Iwasa, Biophys. J. **82**, 1254 (2002).